Scientific Research Publishing

World Journal of Condensed Matter Physics, 2026, 16(4), 236-250
https://www.scirp.org/journal/wjcmp
ISSN Online: 2160-6927
ISSN Print: 2160-6919

Shape- and Size-Dependent Thermoelastic Trends in $FeCoCrNi_2Al$ High-Entropy Alloy: A Literature-Benchmarked Nanothermodynamic Model

Sonal Swaraj, Pinky Kumari, Rupam Kumari, Jagdhar Mandal, Sneha Bharti*

University Department of Physics, Tilka Manjhi Bhagalpur University, Bhagalpur, India
Email: sonalswaraj91@gmail.com, rupam100.patel@gmail.com, pinky123jmt@gmail.com, jmandal1284@gmail.com, *snehachoudhary2906@gmail.com

How to cite this paper: Swaraj, S., Kumari, P., Kumari, R., Mandal, J. and Bharti, S. (2026) Shape- and Size-Dependent Thermoelastic Trends in $FeCoCrNi_2Al$ High-Entropy Alloy: A Literature-Benchmarked Nanothermodynamic Model. *World Journal of Condensed Matter Physics*, **16**, 236-250.
https://doi.org/10.4236/wjcmp.2026.164013

Received: October 7, 2026
Accepted: November 24, 2026
Published: November 27, 2026

Copyright © 2026 by author(s) and Scientific Research Publishing Inc.
This work is licensed under the Creative Commons Attribution International License (CC BY 4.0).
http://creativecommons.org/licenses/by/4.0/

Open Access

Abstract

A geometry-dependent nanothermodynamic formulation is applied to $FeCoCrNi_2Al$ high-entropy alloy (HEA) using published bulk data as a reference. The literature reports a dual FCC+BCC structure, a melting temperature of 1430˚C, and average coefficients of thermal expansion (CTE) of $15.47 \pm 0.20 \times 10^{-6}$ K^{-1} up to 800˚C and $16.23 \pm 0.30 \times 10^{-6}$ K^{-1} up to 1000˚C. The published third-order linear-expansion polynomial is differentiated to reconstruct a temperature-dependent CTE baseline; this is a literature-derived curve, not a new measurement. A surface-atom-fraction model is then used to examine normalized thermal expansion, bulk modulus and cohesive-energy contributions for spherical particles, nanowires and nanofilms. Within the adopted geometric expressions, the predicted surface correction is largest for spheres, intermediate for nanowires and smallest for nanofilms. This ordering is a consequence of the selected geometry model and is not an experimentally established ranking for $FeCoCrNi_2Al$. The comparison between the published melting point (1430˚C) and a rule-of-mixtures estimate (1419˚C; difference 11˚C, approximately 0.77%) is treated only as literature benchmarking. No independent experimental dataset is available to validate the nanoscale predictions. Accordingly, the results are presented as normalized theoretical trends, with explicit limitations arising from the homogeneous-material approximation and the absence of phase-resolved nanoscale elastic data.

Keywords

High-Entropy Alloy, $FeCoCrNi_2Al$, Nanothermodynamics, Thermal Expansion, Bulk Modulus, Cohesive Energy, Surface-Atom Fraction, Shape Effect, Literature Benchmarking

1. Introduction

High-entropy alloys (HEAs) are a class of multicomponent metallic materials generally composed of five or more principal elements in equiatomic or near-equiatomic proportions. Unlike conventional alloys, in which one or two elements usually dominate the composition, HEAs exhibit a complex chemical environment in which configurational entropy, mixing enthalpy, atomic-size mismatch, electronic structure and processing history collectively influence their phase stability and physical properties. These characteristics make HEAs attractive for applications involving elevated temperature, thermal cycling, wear, oxidation and structural loading. The fundamental concepts and development of HEAs have been extensively discussed by Tsai and Yeh, Tsai, and Miracle and Senkov [1]-[3]. The oxidation resistance of FeCoCrNiAl- and $FeCoCrNi_2Al$-based HEAs has also been investigated, demonstrating the relevance of composition and minor-element additions to environmental performance [4].

Among the different classes of HEAs, $FeCoCrNi_2Al$ is particularly interesting because of its experimentally observed multiphase character and measurable high-temperature thermoelastic response. The alloy exhibits a dual FCC+BCC structure, with a reported FCC lattice parameter of approximately 3.57 - 3.58 Å and BCC lattice parameter of approximately 2.87 Å [5]. Jadhav *et al.* investigated $FeCoCrNi_2Al$ using in-situ high-temperature X-ray diffraction (HT-XRD), dilatometry and differential scanning calorimetry (DSC). Their results demonstrated the coexistence of FCC and BCC phases up to 1000˚C, with BCC fractions of approximately 29%, 28% and 30% at 800, 900 and 1000˚C, respectively [6]. The reported average coefficient of thermal expansion (CTE) was $15.47 \pm 0.20 \times 10^{-6}\ K^{-1}$ from room temperature to 800˚C and $16.23 \pm 0.30 \times 10^{-6}\ K^{-1}$ to 1000˚C [7].

Thermal expansion is selected as one of the principal properties because it directly describes the dimensional response of a material to temperature. This property is particularly important for $FeCoCrNi_2Al$ in high-temperature and thermal-barrier-related environments, where thermal-expansion mismatch can generate stresses, dimensional instability and interfacial degradation [8]. The experimentally reported change in thermal-expansion behaviour at elevated temperature also provides a useful bulk benchmark for the present theoretical treatment [7]. General treatments of size- and temperature-dependent thermoelastic properties provide context for interpreting such normalized trends [9] [10].

The bulk modulus is selected as the principal mechanical descriptor because it represents resistance to uniform volumetric deformation and therefore provides a measure of volumetric stiffness. Within the adopted nanothermodynamic framework, the bulk modulus is directly connected to the surface-atom fraction and cohesive-energy correction. As the characteristic dimension decreases, the relative surface contribution increases, leading to a predicted reduction in normalized bulk modulus. Thus, the bulk modulus provides the mechanical interpretation of the nanoscale size effect. Size-dependent thermoelastic behaviour has been examined in previous nanomaterial models [9] [11].

Cohesive energy is included as the energetic descriptor because it provides the physical basis for understanding changes in atomic bonding and effective stiffness at reduced dimensions. Surface atoms have a different bonding environment from atoms in the bulk; therefore, increasing surface fraction lowers the effective cohesive-energy contribution in the adopted model. Cohesive energy consequently links the geometrical surface effect to the predicted mechanical response. The size dependence of nanoparticle cohesive energy has been discussed in earlier theoretical work [8] [12].

Surface-atom fraction is selected as the central geometrical variable because it provides the direct connection between characteristic size, shape and nanoscale response. For a bulk material, surface atoms represent a negligible fraction of the total atoms, whereas reducing a characteristic dimension increases the surface-to-volume ratio. The adopted formulation gives different surface fractions for spherical particles, nanowires and nanofilms, allowing the shape dependence of the predicted thermoelastic properties to be examined within one framework. Related studies have considered shape and size effects in nanomaterial thermophysical properties [9] [13].

The lattice parameter is considered because it provides a crystallographic representation of volumetric expansion. For the cubic relation adopted here, $V \propto a^3$ and therefore $a/a_0 = \left(V/V_0\right)^{1/3}$. This relation connects the macroscopic volumetric response of the equation-of-state treatment with a crystallographic length scale and is particularly relevant to $FeCoCrNi_2Al$ because experimentally reported FCC and BCC lattice parameters are available [5] [7]. Size- and temperature-dependent lattice-parameter trends have also been treated in the nanomaterials literature [9] [11].

The reported melting temperature of 1430˚C and the rule-of-mixtures estimate of 1419˚C differ by 11˚C (approximately 0.77%). This agreement is a comparison between published values and is used here as a literature benchmark only. It does not validate the size- and shape-dependent predictions, for which independent nanoscale experimental data are not available [6]. Size-dependent melting-temperature estimates for metallic nanoparticles provide additional theoretical context, although they do not validate the present alloy-specific nanoscale curves [12].

The analysis therefore separates three evidence levels: published bulk measurements, a reconstructed temperature-dependent curve derived from a published polynomial, and normalized predictions generated by the adopted geometry model. The alloy-specific contribution is the application of this framework to the published $FeCoCrNi_2Al$ bulk baseline and the identification of the data needed for a phase-resolved extension. The geometric equations themselves are general model assumptions and are not unique to this alloy. Earlier work on size-dependent thermoelastic and shape-dependent high-entropy-alloy nanostructures provides broader context for this modelling approach [9]-[11] [13].

The cited $FeCoCrNi_2Al$ studies establish bulk thermal stability and thermal expansion but do not report geometry-resolved nanoscale thermoelastic measurements. Related work has also examined the oxidation resistance of FeCoCrNiAl-

and $FeCoCrNi_2Al$-based high-entropy alloys [4]. The present work applies a generalized surface-fraction model to normalized properties for spheres, nanowires and nanofilms. The resulting curves are theoretical model outputs, not experimentally validated nanoscale properties.

2. Material and Experimental Baseline

The bulk reference is taken from Jadhav *et al.* [7], who prepared $FeCoCrNi_2Al$ from high-purity (>99.5%) Fe, Co, Cr, Ni and Al powders (reported average particle size approximately 45 μm) by mechanical activated synthesis, followed by consolidation by hot pressing. The reported sintered specimen had approximately 97% relative density. In-situ high-temperature X-ray diffraction and dilatometry were conducted from room temperature to 1000˚C; differential scanning calorimetry was performed during heating at 20˚C min^{-1} from 30˚C to 1500˚C under argon. The paper reports a single endothermic peak at 1430˚C. The approximately 3% porosity in the sintered specimen can influence measured bulk expansion and makes direct transfer to idealized, fully dense nanostructures uncertain. These processing and measurement conditions are contextual information from the cited study, not experiments performed in the present work.

Property	Published value
Alloy	$FeCoCrNi_2Al$
Room-temperature phases	FCC + BCC
FCC lattice parameter	≈ 3.57 - 3.58 Å
BCC lattice parameter	≈ 2.87 Å
Melting temperature	1430˚C
Rule-of-mixtures melting temperature	1419˚C
CTE, RT-800˚C	$15.47 \pm 0.20 \times 10^{-6}\ K^{-1}$
CTE, RT-1000˚C	$16.23 \pm 0.30 \times 10^{-6}\ K^{-1}$
BCC fraction at 800˚C	≈ 29%
BCC fraction at 900˚C	≈ 28%
BCC fraction at 1000˚C	≈ 30%
Sintered relative density	≈ 97%

An independent 2019 coating study also reported a major FCC phase and a minor BCC phase, with FCC lattice constant 3.570 ± 0.002 Å and BCC lattice constant 2.87 ± 0.002 Å [5]. These independent values support the use of $FeCoCrNi_2Al$ as a multiphase bulk reference system.

3. Theoretical Formulation

The equations below define the model used to generate normalized trends. The surface-fraction treatment and the size dependence of cohesive energy follow established nanothermodynamic approaches [8] [12], while shape- and

temperature-dependent treatments of thermal expansion, lattice parameter and elastic properties have also been reported [9]-[11]. A related theoretical study of shape- and size-dependent thermophysical and thermoelastic behaviour in high-entropy-alloy nanostructures provides additional context [13]. We distinguish the temperature-dependent bulk reference reconstructed from published data from the general geometry-dependent surface corrections. The manuscript does not perform a numerical pressure sweep: pressure appears only as a formal argument in the equation-of-state expression in **Equation (1)**.

3.1. Equation-of-State Framework

$$\left(V/V_0\right)-1=F\left(P,T,B_0,B_0',\alpha_n\right) \tag{1}$$

Equation (1) is shown as a general equation-of-state placeholder. Because the supplied material does not specify a closed-form function F or provide the required temperature- and pressure-dependent parameters, **Equation (1)** is not numerically evaluated in this study. No pressure-dependent calculations or pressure-resolved predictions are therefore claimed.

3.2. Cohesive Energy and Bulk Modulus

$$E\square^N = E_0\left[1-3N/\left(4n\right)\right] \tag{2}$$

Equation (2) expresses the nanoscale cohesive-energy contribution in terms of the bulk cohesive energy and surface-atom fraction. The normalized cohesive contribution decreases as N/n increases and approaches the bulk value in the large-size limit. This form is consistent with the general size-dependent cohesive-energy treatment reported for nanoparticles [8] [12].

$$B_n = B_0\left[1-3N/\left(4n\right)\right] \tag{3}$$

Equation (3) gives the size-dependent bulk modulus using the same surface correction. The model therefore predicts reduced effective volumetric stiffness as the relative surface contribution increases.

3.3. Geometry-Dependent Surface-Atom Fraction

$$N/n = 4d/D \quad \text{(sphere)} \tag{4}$$

$$N/n = 8d/\left(3D\right) \quad \text{(nanowire)} \tag{5}$$

$$N/n = 4d/\left(3h\right) \quad \text{(nanofilm)} \tag{6}$$

Here, d is an atomic-scale characteristic length, D is the particle or nanowire characteristic diameter, and h is the nanofilm thickness. The expressions are adopted geometric approximations. Their coefficients determine the relative surface contribution within this model; they should not be interpreted as a phase-resolved description of the real alloy microstructure.

3.4. Size-Dependent Thermal Expansion

$$\alpha_n = \alpha_0\left[1-3N/\left(2n\right)\right]^{-1} \tag{7}$$

Equation (7) defines the size-dependent thermal-expansion coefficient. Increasing surface fraction enhances α_n relative to the bulk coefficient α_0 within the adopted model; consequently, decreasing characteristic size produces an increasing normalized thermal-expansion response. Similar size- and temperature-dependent thermal-expansion treatments have been discussed for nanomaterials [9] [10].

3.5. Lattice-Parameter-Volume Relation

$$a/a_0 = \left(V/V_0\right)^{1/3} \tag{8}$$

Equation (8) follows from the cubic relation $V \propto a^3$ and provides a direct conversion from normalized volumetric response to normalized lattice-parameter response. The dependence of lattice parameter on size and temperature has been considered in prior nanomaterial studies [9] [11].

3.6. Temperature-Dependent CTE Reconstruction

The published work fitted linear expansion from 30˚C to 1000˚C with a third-order polynomial [4]. The coefficients are literature-derived; therefore, the following relation is a reconstructed representation rather than a new experimental fit.

$$\Delta L/L_0 = AT^3 + BT^2 + CT + D \tag{9}$$

The coefficients are $A = -1.097 \times 10^{-12}$, $B = 5.550 \times 10^{-9}$, $C = 1.160 \times 10^{-5}$ and $D = -2.987 \times 10^{-4}$.

$$\alpha_{\text{poly}}\left(T\right) = 3AT^2 + 2BT + C \tag{10}$$

Equation (10) is obtained by differentiating **Equation (9)** with respect to temperature and represents the instantaneous polynomial-derived CTE over the fitted temperature range.

3.7. Normalized Nanoscale Relations

The normalized treatment avoids assigning unsupported absolute nanoscale values. For the plotted dimensionless characteristic size x, $x = D/d$ for spheres and nanowires and $x = h/d$ for nanofilms. The displayed curves span the dimensionless range of $x = 7$ - 200, with the large-x limit representing bulk-like behaviour. The equations are evaluated using the surface-fraction expressions in **Equations 13(a)-(c)**, consistent with theoretical treatments of shape- and size-dependent thermoelastic properties [9]-[11] [13]. The thermal-expansion expression contains a denominator that approaches zero at sufficiently small x; results near that singular region are not physically reliable and should not be interpreted quantitatively. The figures are therefore used to illustrate model trends, not to establish a validated minimum particle size. No pressure-dependent calculations were performed.

Calculation protocol. The geometry curves use the dimensionless size $x = D/d$

(sphere and nanowire) or $x = h/d$ (nanofilm), over $x = 7$ - 200. The expressions were evaluated at integer values of x from 7 through 200 and connected to display smooth model curves; these are not experimental points. The bulk temperature dependence enters only through the literature-derived $\alpha_0(T)$ baseline reconstructed from **Equations (9)-(10)**; the normalized size corrections are then applied through N/n. No pressure sweep was performed, and **Equation (1)** was not numerically solved. Because **Equation (11)** becomes singular when its denominator approaches zero, the smallest-size portion should be treated as a mathematical extrapolation and not as a physically reliable prediction. A rigorous numerical study should restrict the domain to a physically admissible interval and regenerate the plots accordingly.

$$\alpha_n/\alpha_0 = \left[1-3N/(2n)\right]^{-1} \tag{11}$$

$$B_n/B_0 = 1-3N/(4n) \tag{12}$$

Both relations approach unity in the large-size limit. **Equation (11)** increases above unity as surface fraction increases, whereas **Equation (12)** decreases below unity as surface fraction increases.

$$N/n = 4d/D \quad \text{(sphere)} \tag{13a}$$

$$N/n = 8d/(3D) \quad \text{(nanowire)} \tag{13b}$$

$$N/n = 4d/(3h) \quad \text{(nanofilm)} \tag{13c}$$

$$E^N/E_0 = 1-3N/(4n) \tag{14}$$

3.8. Proposed Phase-Weighted Extension

$$\alpha_{\text{eff}}(T,D) = f_{\text{FCC}}(T)\alpha_{\text{FCC}}(T,D) + f_{\text{BCC}}(T)\alpha_{\text{BCC}}(T,D) \tag{15}$$

Equation (15) is a proposed extension rather than a calculation performed here. The available BCC fractions at 800˚C, 900˚C and 1000˚C are discrete reference points; a continuous phase-fraction function would require the original Rietveld data or an independently validated CALPHAD calculation.

4. Results and Discussion

Results are organized in the order of the figures. Figure 1 presents the bulk melting-temperature benchmark, and Figure 2 shows the reconstructed literature-based CTE curve. Figures 3-6 then present normalized predictions from the adopted geometry model, while Figure 7 shows the normalized lattice-parameter-volume consistency relation. Only the bulk measurements and literature-derived baseline are based on published experimental work; the nanoscale model outputs do not represent independent experimental validation.

4.1. Literature Benchmark of Melting Temperature

The published melting temperature is 1430˚C, while the rule-of-mixtures estimate is 1419˚C. The 11˚C difference corresponds to approximately 0.77% relative to the

reported experimental value. This close numerical agreement is a literature benchmark between two bulk values; it is not a validation of the nanoscale model.

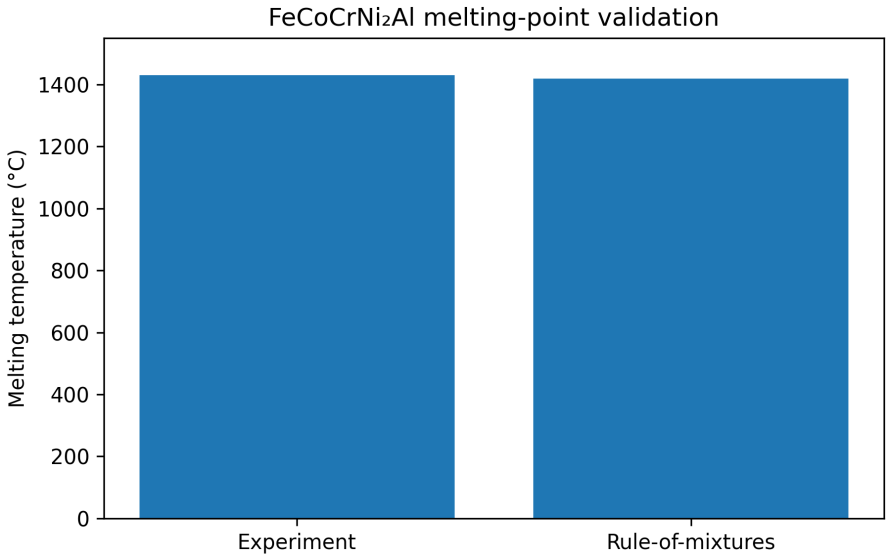

Figure 1. Literature-reported melting temperature (1430˚C) compared with the rule-of-mixtures estimate (1419˚C); the comparison is a bulk literature benchmark, not validation of nanoscale predictions.

4.2. Temperature-Dependent Thermal-Expansion Baseline

The reconstructed instantaneous CTE obtained by differentiating the published third-order expansion polynomial increases from approximately 11.93×10^{-6} K^{-1} at 30˚C to 19.41×10^{-6} K^{-1} at 1000˚C. The corresponding values at 30, 200, 400, 600, 800 and 1000˚C are approximately 11.93, 13.69, 15.51, 17.08, 18.37 and 19.41×10^{-6} K^{-1}, respectively.

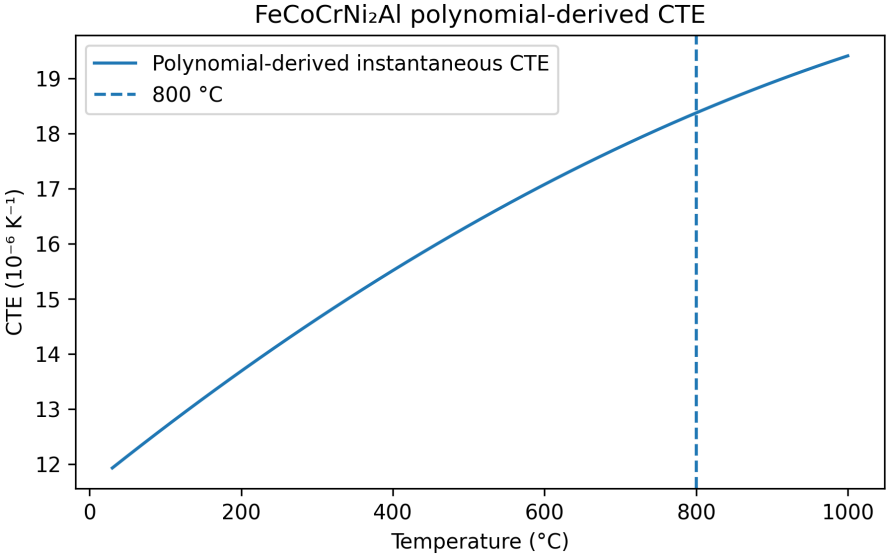

Figure 2. CTE reconstructed from the published third-order linear-expansion fit; this is a model curve, not newly measured experimental data [4].

The derivative of the published third-order expansion polynomial rises from approximately 11.93×10^{-6} K^{-1} at 30˚C to 19.41×10^{-6} K^{-1} at 1000˚C. These are reconstructed instantaneous values. They should not be directly equated with the reported average CTE values over RT-800˚C and RT-1000˚C, because the quantities are defined differently. The original raw expansion data would be required for an independent residual or uncertainty analysis.

4.3. Normalized Thermal Expansion: Geometry and Size Effect

The model predicts an increase in normalized CTE as the characteristic dimension decreases. This follows from the inverse dependence on the adopted surface fraction and is qualitatively consistent with published theoretical treatments of size- and shape-dependent thermal expansion [9]-[11] [13]. The relative separation between the curves is imposed by the coefficients in **Equations (4)-(6)**, rather than by measured alloy-specific surface energetics. The ranking should therefore be read as a property of the chosen geometric parameterization.

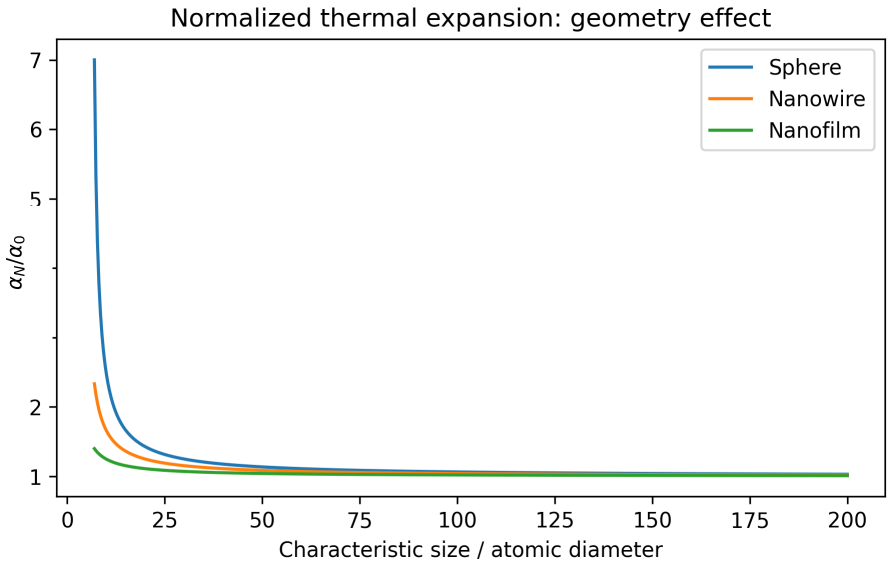

Figure 3. Predicted normalized thermal-expansion coefficient α_n/α_0 versus characteristic size/atomic diameter for sphere, nanowire and nanofilm geometries [9]-[11] [13].

4.4. Normalized Bulk Modulus: Geometry and Size Effect

The normalized bulk-modulus relation decreases with increasing surface fraction. It is a direct consequence of **Equation (12)**, not an independent prediction from phase-specific elastic constants. Because $FeCoCrNi_2Al$ contains FCC and BCC phases, the single effective modulus used here cannot represent distinct phase stiffnesses or mechanical coupling between the phases.

4.5. Normalized Cohesive Energy: Energetic Size Effect

The cohesive-energy contribution follows the same surface-fraction correction as the normalized bulk modulus in the adopted equations. **Figure 5** is therefore

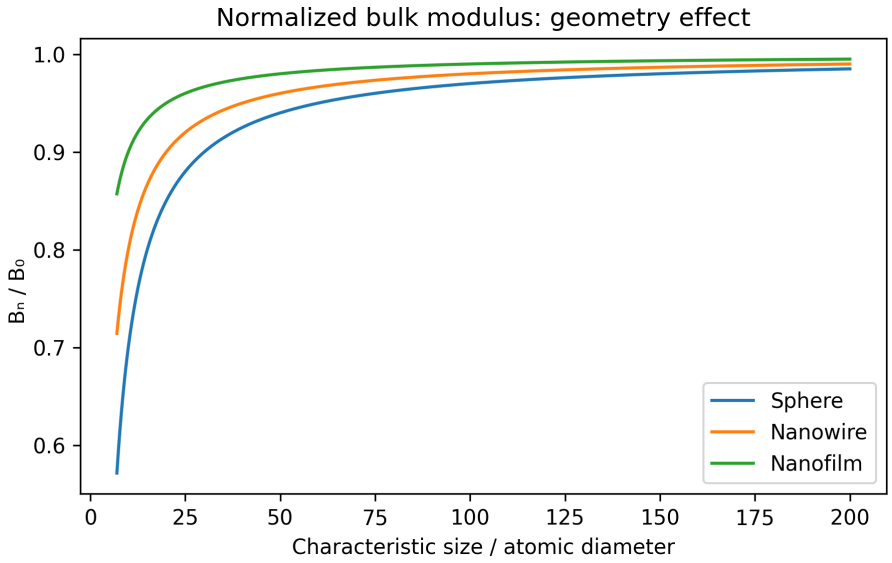

Figure 4. Predicted normalized bulk modulus B_n/B_0 versus characteristic size/atomic diameter for the three geometries [9] [10] [13].

mathematically linked to **Figure 4** rather than providing an independent energetic validation. Its interpretation is limited to the model's normalized cohesive-energy term, consistent with general size-dependent cohesive-energy approaches [8] [12].

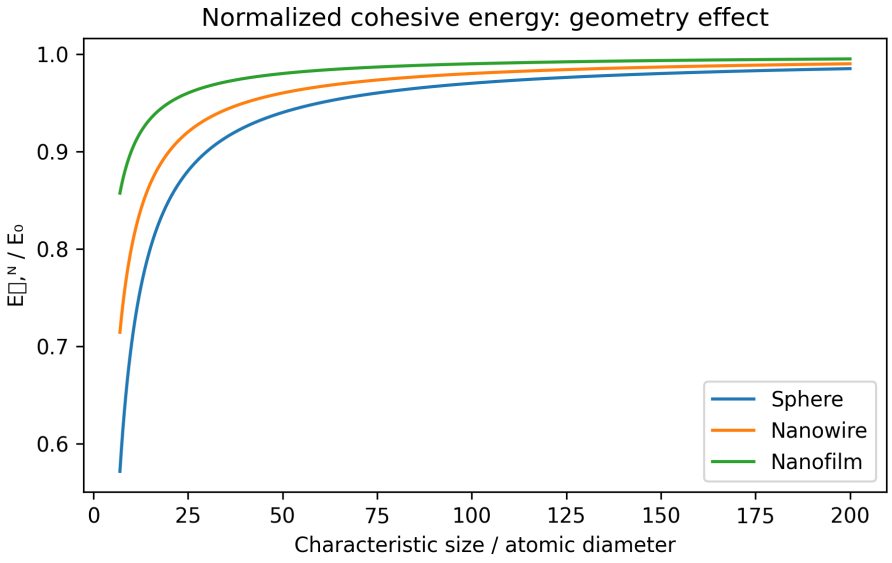

Figure 5. Predicted normalized cohesive energy E^{N}/E_0 versus characteristic size/atomic diameter for sphere, nanowire and nanofilm geometries [8] [12].

4.6. Surface-Atom Fraction: Geometric Origin of the Size Effect

The surface-atom fraction is the model's common geometric input. It decreases with increasing characteristic size and sets the relative magnitude of the corrections in **Equations (11)-(14)**. This relationship explains the model-generated separation among geometries and is consistent with surface-fraction approaches used

in nanothermodynamic models [8]-[13]; it does not establish the actual surface composition or atomic coordination of $FeCoCrNi_2Al$ nanostructures.

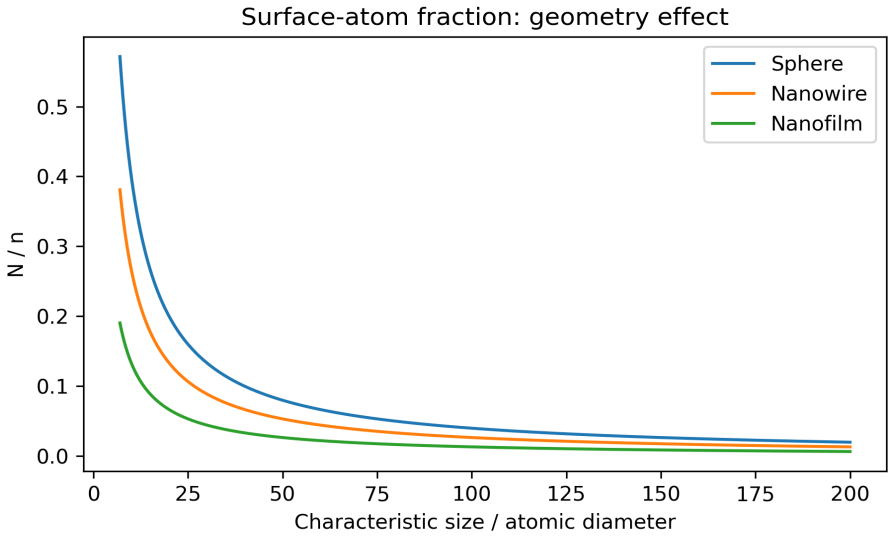

Figure 6. Predicted surface-atom fraction N/n versus characteristic size/atomic diameter for sphere, nanowire and nanofilm geometries [10] [13].

4.7. Normalized Lattice-Parameter-Volume Coupling

Equation (8) is the cubic crystallographic relation between normalized volume and lattice parameter. **Figure 7** is a parameter-free mathematical consistency plot, not an independently calculated or measured $FeCoCrNi_2Al$ response.

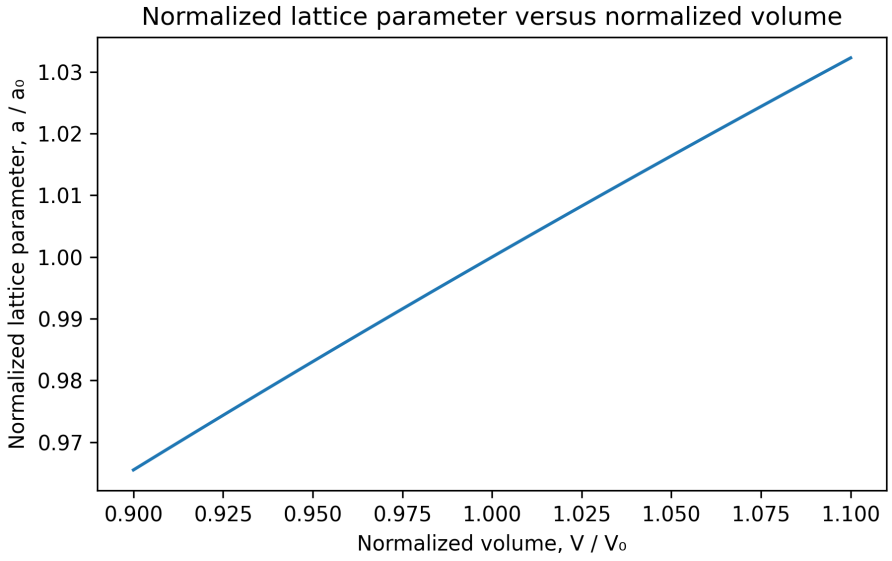

Figure 7. Normalized lattice parameter a/a_0 versus normalized volume V/V_0 obtained from **Equation (8)**; this is a model consistency relation, not an independent experimental dataset [9] [11].

4.8. Integrated Interpretation

Figures 1-2 provide bulk literature context: **Figure 1** compares two reported bulk

melting-temperature values, while Figure 2 reconstructs the instantaneous CTE from the published polynomial. Figures 3-6 show the consequences of the adopted surface-fraction model for normalized CTE, bulk modulus, cohesive-energy contribution and surface fraction. Figure 7 expresses the cubic relation between normalized volume and lattice parameter. Only the bulk information is literature-derived; the nanoscale curves are model predictions and have not been independently tested against nanoscale measurements.

At equal dimensionless size, the adopted equations give the largest surface correction for a sphere, followed by a nanowire and a nanofilm. This ordering is not a universal experimental law: it follows from the coefficients chosen for the idealized geometries and could change if aspect ratio, faceting, surface reconstruction, phase distribution or composition-dependent surface energies were included.

The model's principal analytical result is the internally consistent mapping from surface fraction to normalized properties: increasing N/n lowers the model's cohesive-energy and bulk-modulus terms while raising the normalized CTE term. These linked trends are consequences of the selected equations and should not be treated as independent confirmations of one another. The geometry-specific surface-fraction expressions and their relative corrections are summarized in the table below.

Geometry	Surface fraction N/n	Predicted relative correction
Sphere	4 d/D	Strongest surface correction
Nanowire	8 d/(3 D)	Intermediate surface correction
Nanofilm	4 d/(3 h)	Weakest surface correction at the same dimensionless size

5. Scientific Contribution and Novelty

- Published $FeCoCrNi_2Al$ bulk data provide the alloy-specific reference state; no new measurements are reported.
- The general surface-fraction equations are applied to the $FeCoCrNi_2Al$ reference to obtain normalized, geometry-dependent trends; the equations themselves are material-general.
- The comparison among sphere, nanowire and nanofilm quantifies the consequences of the adopted geometric coefficients, not a measured alloy-specific shape ranking.
- The manuscript distinguishes published measurements, reconstructed literature-derived curves and theoretical model outputs.
- A phase-weighted extension is formulated for future work but is not numerically evaluated here.
- Normalization avoids unsupported absolute nanoscale constants, while also limiting the conclusions to relative model trends.

6. Limitations and Scope for Quantitative Extension

Several limitations constrain interpretation. First, the nanoscale predictions have not been compared with independent experimental measurements and must not

be described as validated. Second, the homogeneous-material approximation omits phase-specific FCC and BCC stiffness, mechanical constraints and load transfer between coexisting phases, and possible surface segregation or composition-dependent surface energies. Consequently, the predicted shape ranking cannot establish which real $FeCoCrNi_2Al$ nanostructure is mechanically or thermally superior. Third, the bulk experimental reference was obtained from a sintered specimen with approximately 97% relative density; porosity can affect measured expansion and limits direct comparison with idealized dense structures. Fourth, the equations do not include a numerical pressure dependence, and the equation-of-state function in **Equation (1)** is not evaluated. Finally, the small-size limit of the thermal-expansion expression contains a singular denominator, so results near that region are not physically interpretable. Quantitative validation would require phase-resolved bulk parameters, a clearly specified size-validity range, original bulk datasets and independent nanoscale measurements.

Future work should obtain the original temperature-dependent lattice and phase-fraction data, phase-specific elastic constants, and nanoscale measurements or validated atomistic/CALPHAD calculations. Those data would permit a phase-weighted treatment and quantitative metrics such as RMSE or MAE. Until then, the current curves should be interpreted as model-based normalized trends rather than quantitatively validated predictions.

7. Conclusions

- Published studies report a melting temperature of 1430˚C for $FeCoCrNi_2Al$ and a rule-of-mixtures estimate of 1419˚C. Their approximately 0.77% difference is a literature benchmark only; it does not validate nanoscale predictions.
- Differentiation of the published expansion polynomial reconstructs an instantaneous CTE increasing from approximately 11.93×10^{-6} K^{-1} at 30˚C to 19.41×10^{-6} K^{-1} at 1000˚C. This reconstructed curve is distinct from the published average CTE values.
- The normalized geometry model predicts that increasing surface fraction raises its CTE term and lowers its cohesive-energy and bulk-modulus terms. These linked trends follow from the adopted equations.
- The sphere-nanowire-nanofilm ranking reflects the coefficients in the idealized geometric expressions; it is not an experimentally demonstrated ranking for $FeCoCrNi_2Al$.
- The alloy-specific contribution is the application of a general model to the published $FeCoCrNi_2Al$ bulk reference and the explicit identification of information required for a phase-resolved extension.
- Because nanoscale measurements are absent and the model omits phase-specific stiffness, FCC/BCC mechanical coupling and surface segregation, the results should be treated as theoretical trends, not validated nanoscale properties.
- The normalized volume-lattice-parameter relation is a mathematical consistency

relation and does not constitute independent experimental evidence.

- Overall, the study provides a literature-benchmarked, shape-resolved theoretical analysis, with its assumptions and limits stated explicitly.

Author Contributions

Conceptualisation: Jagdhar Mandal; Methodology: Pinky Kumari; Analysis: Sonal Swaraj; Writing, Review and Editing: Rupam Kumari & Sneha Bharti; Investigation: Pinky Kumari & Sonal Swaraj; Validation & Supervision: Jagdhar Mandal; Corresponding Author: Sneha Bharti.

Conflicts of Interest

The authors declare no conflicts of interest regarding the publication of this paper.

References

[1] Tsai, M. and Yeh, J. (2014) High-Entropy Alloys: A Critical Review. *Materials Research Letters*, **2**, 107-123. https://doi.org/10.1080/21663831.2014.912690

[2] Tsai, M. (2013) Physical Properties of High Entropy Alloys. *Entropy*, **15**, 5338-5345. https://doi.org/10.3390/e15125338

[3] Miracle, D.B. and Senkov, O.N. (2017) A Critical Review of High Entropy Alloys and Related Concepts. *Acta Materialia*, **122**, 448-511. https://doi.org/10.1016/j.actamat.2016.08.081

[4] Jadhav, M., Singh, S., Srivastava, M., Chethan, Chakradhar, R.P.S. and Panigrahi, B.B. (2022) Effect of Minute Element Addition on the Oxidation Resistance of FeCoCrNiAl and FeCoCrNi$_2$Al High Entropy Alloy. *Advanced Powder Technology*, **33**, Article 103410. https://doi.org/10.1016/j.apt.2021.103410

[5] Srivastava, M., Jadhav, M., Chethan, Chakradhar, R.P.S., Muniprakash, M. and Singh, S. (2019) Synthesis and Properties of High Velocity Oxy-Fuel Sprayed FeCoCrNi$_2$Al High Entropy Alloy Coating. *Surface and Coatings Technology*, **378**, Article 124950. https://doi.org/10.1016/j.surfcoat.2019.124950

[6] Jadhav, M., Singh, S., Srivastava, M. and Vinod Kumar, G.S. (2019) An Investigation on High Entropy Alloy for Bond Coat Application in Thermal Barrier Coating System. *Journal of Alloys and Compounds*, **783**, 662-673. https://doi.org/10.1016/j.jallcom.2018.12.361

[7] Jadhav, M.S., Sahane, D., Verma, A. and Singh, S. (2021) Thermal Stability and Thermal Expansion Behavior of FeCoCrNi$_2$Al High Entropy Alloy. *Advanced Powder Technology*, **32**, 378-384. https://doi.org/10.1016/j.apt.2020.12.019

[8] Qi, W.H. and Wang, M.P. (2002) Size Effect on the Cohesive Energy of Nanoparticle. *Journal of Materials Science Letters*, **21**, 1743-1745. https://doi.org/10.1023/a:1020904317133

[9] Goyal, M. and Gupta, B.R.K. (2018) Shape, Size and Temperature Dependency of Thermal Expansion, Lattice Parameter and Bulk Modulus in Nanomaterials. *Pramana*, **90**, Article 80. https://doi.org/10.1007/s12043-018-1563-8

[10] Kumar, R., Sharma, G. and Kumar, M. (2013) Size and Temperature Effect on Thermal Expansion Coefficient and Lattice Parameter of Nanomaterials. *Modern Physics Letters B*, **27**, Article 1350180. https://doi.org/10.1142/s0217984913501807

[11] Kumar, R. and Kumar, M. (2010) Size Dependence of Thermoelastic Properties of

Nanomaterials. *International Journal of Nanoscience*, **9**, 537-542. https://doi.org/10.1142/s0219581x10007113

[12] Qu, Y.D., Liang, X.L., Kong, X.Q. and Zhang, W.J. (2017) Size-Dependent Cohesive Energy, Melting Temperature, and Debye Temperature of Spherical Metallic Nanoparticles. *Physics of Metals and Metallography*, **118**, 528-534. https://doi.org/10.1134/s0031918x17060102

[13] Kumari, P., Swaraj, S., Kumar, M., Kumar, K., Vrind, N. and Mandal, J. (2026) Size- and Shape Dependent Thermophysical and Thermoelastic Properties of High-Entropy Alloy CoCrFeMnNi Nanostructures. *World Journal of Condensed Matter Physics*, **16**, 138-160.